RSC Advances

ROYAL SOCIETY OF CHEMISTRY

PAPER

View Article Online
View Journal | View Issue

Check for updates

Cite this: *RSC Adv.*, 2020, **10**, 38592

New Span-PEG-composited Fe_3O_4-CNT as a multifunctional ultrasound contrast agent for inflammation and thrombotic niduses

Jie Zhang,[*a] Jinzi Yang,[a] Huiming Zhang,[b] Ming Hu,[*c] Jinjing Li[a] and Xiangyu Zhang[a]

Received 22nd June 2020
Accepted 25th September 2020

DOI: 10.1039/d0ra05401a

rsc.li/rsc-advances

By attaching ferroferric oxide (Fe_3O_4) to drug-carrying carbon nanotubes (CNTs), we generated a new Span-PEG composite with Fe_3O_4-CNT multifunctional microbubbles for inflammation and thrombus niduses. The Fe_3O_4-CNT magnetic targeting complex was prepared by *in situ* synthesis, and then acetylsalicylic acid (ASA) and gentamicin (GM) were loaded onto the Fe_3O_4-CNT complex by physical methods to produce Fe_3O_4-CNT-ASA and Fe_3O_4-CNT-GM complexes, respectively. Span-PEG-composited Fe_3O_4-CNT-ASA or Fe_3O_4-CNT-GM microbubbles were synthesized with Span and PEG as the membrane materials by the acoustic cavitation method. The obtained composite microbubbles were smooth, hollow spheres with an average particle size of 425 nm. The ASA and GM loading rates in Span-PEG-composited Fe_3O_4-CNT-ASA and Fe_3O_4-CNT-GM microbubbles were 1.12% and 19.05%, respectively. Span-PEG-composited Fe_3O_4-CNT-ASA microbubbles inhibited thrombosis and demonstrated an anticoagulation effect *in vitro*. Additionally, Span-PEG-composited Fe_3O_4-CNT-ASA microbubbles showed significantly enhanced ultrasound imaging of rabbit abdominal aorta and extended the signal time under the action of an external magnetic field. Thus, Span-PEG-composited Fe_3O_4-CNT-GM microbubbles inhibited *Escherichia coli* and *Staphylococcus aureus*, enhanced the ultrasound imaging of rabbit abdominal uterus and had better stability and fluidity.

1 Introduction

Ultrasound molecular imaging is achieved using targeted microbubble contrast agents, which are highly reflective ultrasound materials that can target specific tissue imaging using specific biomarkers.[1] The imaging of targeted microbubble ultrasound contrast agents in thrombosis and inflammation has attracted increased research attention, and the targeted specificity and binding stability of the contrast agent are beneficial for early diagnosis.[2,3] Thrombus formation is a common condition of the cardiovascular system. For example, deep vein thrombosis is often called a "silent killer" because of the lack of obvious symptoms until the late stage.[4,5] Deep vein thrombosis most often occurs in the legs, but it can gradually invade the deep veins of the arms, visceral veins, and cerebral veins.[6] Therefore, early diagnosis and appropriate treatment are very important to reduce the morbidity and mortality of thrombosis. As a result, ultrasound has become an important detection method presently. Angiography can improve the resolution of the vascular intima, and ultrasound contrast agents can more accurately determine intravascular occlusion and increase measurement accuracy. Johri *et al.*[7] determined the activity of blood flow by observing microbubble movement in intracavitary blood vessels after vasodilation so that intravascular conditions could be observed. Pelvic inflammation is a gynecological disease that threatens women's health. Accurate assessments of the morphology and function of the uterus and fallopian tubes are the keys to diagnosis and treatment. Recently, some studies have shown that microbubble ultrasound contrast agents could be used to assess the patency performance of fallopian tubes; this finding has been increasingly recognized by clinicians and patients in recent years due to their high accuracy, noninvasiveness, and low cost. Dreyer *et al.*[8] conducted a study to explore the influence of the choice of hysterosalpingian tube contrast media on the pregnancy rate. In that study, 1119 women were randomly assigned to use oil-based contrast media or water-based contrast media for hysterosalpingography. The pregnancy rate of women who received oil-based contrast hysterosalpingography was as high as 29.1%, slightly higher than that of women who received water-based contrast hysterosalpingography.

As one of the most advanced nanocarriers for the efficient delivery of drugs, CNTs can achieve transmembrane transportation by noncovalent or covalent binding with different

---

[a] Pharmacy College, Jiamusi University, Jiamusi 154007, China. E-mail: zjie612@163.com; Tel: +86 18045411988

[b] College of Basic Medicine, Jiamusi University, Jiamusi 154007, China

[c] College of Materials Science & Engineering, Jiamusi University, Jiamusi 154007, China. E-mail: minghu02@jmsu.edu.cn; Tel: +86 13846158051

drugs, biomolecules and nanoparticles. Zhang *et al.*[9] prepared a nanometer drug-loaded complex with CNTs covalently binding with the anticancer drug doxorubicin (DOX), significantly improving the drug loading capacity and drug release kinetics; additionally, the obtained CNT-DOX complex showed a multistimulus response induced by pH, temperature and a reducing agent. CNTs are an emerging diagnostic imaging tool. The application of CNTs in ultrasound imaging can enhance the role of ultrasound imaging, increase the drug loading and stability of ultrasound contrast agents, and reduce the burst release of drugs.

Fe_3O_4 nanoparticles have the characteristics of stability, controllability, and strong targeting due to the unique magnetic property and have broad application prospects in the field of biomedicine. Attari *et al.*[10] delivered methotrexate coupled with Fe_3O_4 to cancer cells under the guidance of an external magnetic field, which enhanced the delivery of the therapeutic complex at their action sites.

In this study, the excellent drug-carrying ability and imaging function of CNTs were effectively combined with the superparamagnetic property of Fe_3O_4 nanoparticles, and they were applied as ultrasound contrast agents. A new Span-PEG composited with Fe_3O_4-CNT multifunctional ultrasound contrast agent was obtained that demonstrated multiple effects in ultrasound imaging, targeting and adjuvant therapy by loading ASA and GM onto the Fe_3O_4-CNT complexes, which could be applied to early prevention and intervention in thrombus and inflammation.

2 Experiment

2.1 Preparation of Span-PEG-composited drug-Fe_3O_4-CNT microbubbles

First, 0.45 g of CNTs was dispersed in distilled water under ultrasound and transferred into a three-necked flask. Next, 0.47 g of $FeCl_3$, 0.23 g of $FeCl_2$ and an appropriate amount of PEG1500 were added to this three-necked flask. NaOH solution (4 mg mL^{-1}) was slowly added to the above system at 60 °C until the reaction system was alkaline, stirring for 20 min and aging for 30 min at 80 °C. After the reaction, the sediment was gathered at the bottom of the flask by the magnet, repeatedly washing with triple-distilled water, and the Fe_3O_4-CNT magnetic targeting complex was obtained by freeze-drying.

Second, 20 mg of the Fe_3O_4-CNT complex was dispersed in an appropriate amount of distilled water. Next, 80 mg of gentamicin (GM) and 80 mg of aspirin (ASA) were dissolved in the appropriate amount of distilled water and absolute ethanol, respectively. Additionally, the two obtained drug liquids were added to the Fe_3O_4-CNT suspension, stirring at 30–40 °C for 120–150 min. After the above system was filtered, washed and freeze-dried, the Fe_3O_4-CNT-GM and Fe_3O_4-CNT-ASA complexes were obtained.

Finally, 30 mg of Fe_3O_4-CNT-GM complex and 30 mg of Fe_3O_4-CNT-ASA complex were dispersed into 10 mL of PBS under ultrasound. Next, 450 mg of Span60, 450 mg of PEG1500 and 900 mg of NaCl were ground well and transferred to a beaker with 40 mL of PBS, stirring for 30 min at 80 °C. The above complex dispersion was then added into this system, and the stirring process was continued for 15 min. The obtained mixture was subjected to an ultrasonic cell disruption instrument at a power of 600 W for 6 min, while nitrogen gas was introduced. After washing 3–4 times with PBS, the middle layer of the microbubble suspension was collected and freeze-dried. Finally, Span-PEG-composited Fe_3O_4-CNT-GM and Fe_3O_4-CNT-ASA microbubbles were prepared.

2.2 Determination of the drug content in the composite microbubbles

2.2.1 ASA content in Span-PEG-composited Fe_3O_4-CNT-ASA microbubbles. First, ASA standard liquids at 50 μg mL^{-1}, 100 μg mL^{-1}, 150 μg mL^{-1}, 200 μg mL^{-1} and 250 μg mL^{-1} were prepared using an ASA standard and anhydrous ethanol. Using anhydrous ethanol as the blank, the absorbance of each sample was determined at 276.0 nm and a linear regression equation of ASA was derived.

Span-PEG-composited Fe_3O_4-CNT-ASA microbubbles (50 mg) was dissolved in an appropriate amount of anhydrous ethanol and was treated to release the drug under ultrasound for 2 h. The obtained mixture was filtered using a microporous membrane, and 25 mL of the filtrate was subjected to ultraviolet spectrophotometry at 276.0 nm. According to the ASA standard curve, the loading rate of ASA in the composite microbubbles was calculated.

2.2.2 GM content in Span-PEG-composited Fe_3O_4-CNT-GM microbubbles. To draw the GM standard curve, GM standard liquids of 10 μg mL^{-1}, 25 μg mL^{-1}, 50 μg mL^{-1}, 100 μg mL^{-1}, 200 μg mL^{-1} and 500 μg mL^{-1} were prepared using a GM standard and triple-steamed water. Using triple-steamed water as a blank, the absorbance of each sample was determined at 320.0 nm. The linear regression equation of GM was also obtained.

Span-PEG-composited Fe_3O_4-CNT-GM microbubbles (20 mg) was dissolved in an appropriate amount of triple-steamed water and was treated to release drug under ultrasound for 2 h. The obtained mixture was filtered using a microporous membrane, and 20 mL of the filtrate was subjected to ultraviolet spectrophotometry at 320.0 nm. According to the above method, the loading rate of GM in the composite microbubbles was obtained.

2.3 *In vitro* antibacterial analysis of Span-PEG-composited Fe_3O_4-CNT-GM microbubbles

Physiological saline suspensions of Span-PEG microbubbles, Span-PEG-composited Fe_3O_4-CNT microbubbles, Span-PEG-composited CNT-GM microbubbles and Span-PEG-composited Fe_3O_4-CNT-GM microbubbles were treated under ultrasound to release the drug. Additionally, filter paper was placed into each sample solution and allowed to soak for 12 h.

Drug-sensitive papers of Span-PEG-composited Fe_3O_4-CNT-GM microbubbles at different concentrations and with different composite microbubbles were prepared. Six pieces per drug-sensitive paper were prepared and attached to the surfaces of *Escherichia coli* and *Staphylococcus aureus* agar plates. The plates with the drug-sensitive papers were placed into an incubator at 37 °C for 12 h, and the diameter of the inhibition zone was measured using a Vernier caliper.

2.4 *In vitro* antithrombotic experiment of Span-PEG-composited Fe_3O_4-CNT-ASA microbubbles

As mentioned in section 2.3 of this study, the different microbubble suspension groups were treated to release the drug under ultrasound. Span-PEG microbubbles, Span-PEG-composited CNT microbubbles, Span-PEG-composited Fe_3O_4-CNT microbubbles, Span-PEG-composited CNT-ASA microbubbles and Span-PEG-composited Fe_3O_4-CNT-ASA microbubbles were prepared. Three parallel samples were set for each group, and each tube was fitted with 0.5 mL of blood. The formed clot was removed and weighed after 1 h of drug action.

After different microbubbles interacted with the blood, the following blood coagulation parameters were measured using an automatic blood coagulation analyzer: prothrombin time (PT), activated partial thromboplastin time (APTT), thrombin time (TT) and international normalized ratio (INR).

2.5 Ultrasound imaging of Span-PEG-composited Fe_3O_4-CNT-GM microbubbles

The New Zealand white rabbit was used as an experimental subject. After anesthesia, the uterus of the rabbit was perfused with Span-PEG composited with Fe_3O_4-CNT-GM microbubbles (60 mg mL^{-1}) in physiological saline by uterine intubation. Ultrasound imaging of the rabbit uterus before and after injection was observed and recorded using a Doppler color ultrasound imaging system.

2.6 Ultrasound imaging of Span-PEG-composited Fe_3O_4-CNT-ASA microbubbles

The experimental groups were as follows: normal saline control group, Span-PEG microbubbles, Span-PEG-composited CNT microbubbles and Span-PEG-composited Fe_3O_4-CNT-ASA microbubbles. Freeze-dried powders of different microbubbles were added to the suspensions at a concentration of 60 mg mL^{-1} with degassed physiological saline.

The rabbit abdominal aorta thrombosis model was established. First, filter paper was immersed with 34% ferric chloride aqueous solution. Next, a healthy rabbit was anesthetized according to its weight, and the underbelly hair was shaved. An abdominal aorta section of 2 cm was dissociated by abdominal surgery and covered by the above-treated filter paper to induce the formation of the thrombosis model. Thereafter, the normal saline group and each microbubble suspension group were injected with the materials *via* the marginal ear vein. Ultrasound inspection of the abdominal aorta was performed using a Doppler color ultrasound instrument.

3 Results and discussion

Fig. 1 displays the hysteresis curves of Fe_3O_4-CNT magnetic targeting complexes and Span-PEG-composited Fe_3O_4-CNT microbubbles at room temperature. These two hysteresis curves showed similar magnetic behavior, no coercive magnetic field and remanence at the zero point, indicating that the prepared Fe_3O_4-CNT magnetic targeting complexes and Span-PEG-composited Fe_3O_4-CNT microbubbles had good magnetic properties.

SEM and TEM of Span-PEG-composited Fe_3O_4-CNT microbubbles are shown in Fig. 2. The prepared Span-PEG-composited Fe_3O_4-CNT microbubbles had a smooth surface and a uniform particle size (Fig. 2(a)). Span-PEG-composited Fe_3O_4-CNT microbubbles showed a hollow structure, the size was nanoscale, and the outer membrane layer of the composite microbubbles showed a black shaded area (Fig. 2(b)). Combined with Fig. 2(b), the structure simulation of Span-PEG-composited Fe_3O_4-CNT microbubbles is shown in Fig. 2(c). In the preparation process of composite microbubbles, using water as the dispersing phase, Span and PEG as the surfactant molecules formed stable microbubbles that wrapped N_2 inside the acoustic cavitation. Incidentally, the hydrophilic end of Span was outward while its hydrophobic end was inward, and PEG macromolecules were interspersed among the Span60 molecules. Additionally, due to the hydrophilicity of the carboxylated CNTs in the Fe_3O_4-CNT complex, the Fe_3O_4-CNT complex combined with the outer wall of the composite microbubbles. Under a higher preparation temperature, the

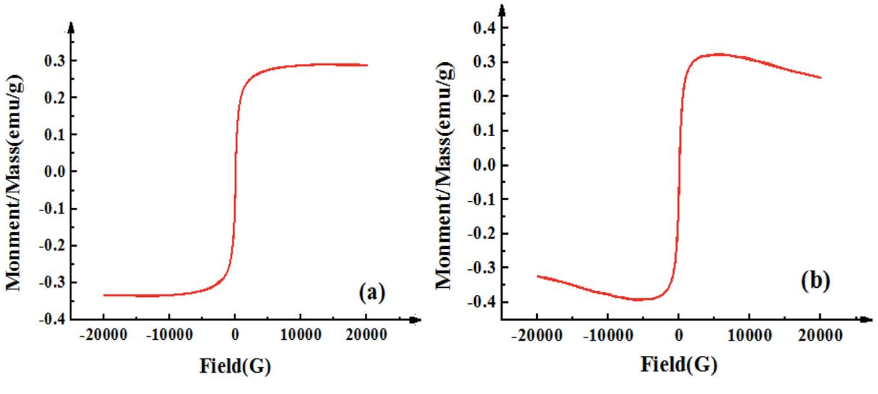

Fig. 1 Hysteresis curves of the Fe_3O_4-CNT complex (a) and Span-PEG-composited Fe_3O_4-CNT microbubbles (b) at room temperature.

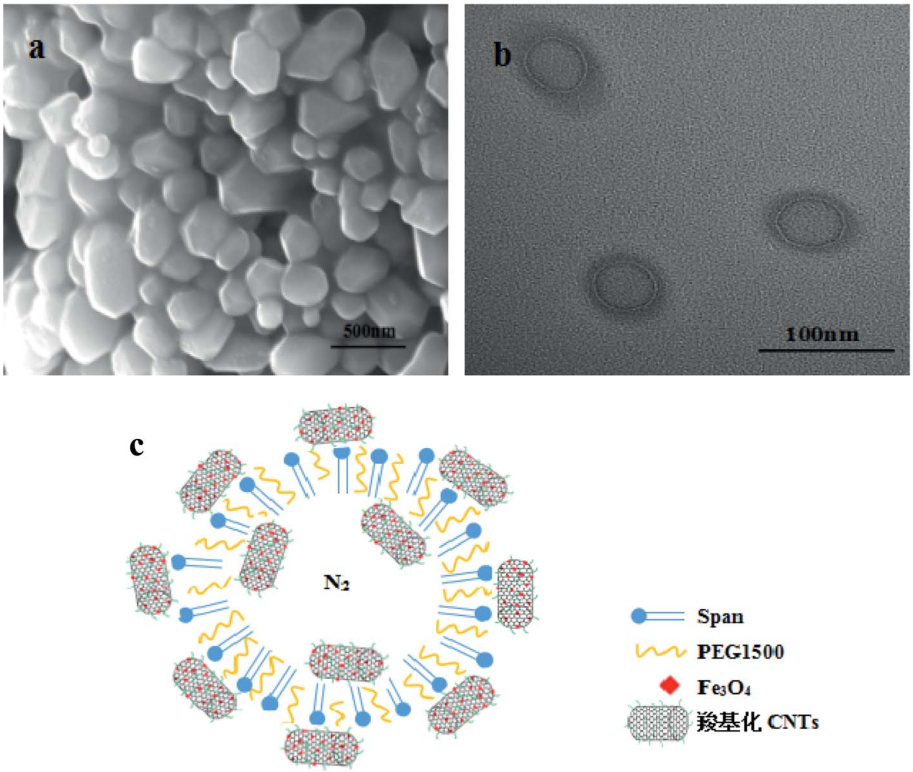

Fig. 2 SEM (a), TEM (b) and structure simulation diagram (c) of Span-PEG-composited Fe_3O_4-CNT microbubbles.

carboxyl group on the Fe_3O_4-CNTs complex could form ester bonds with the hydroxyl group of Span by dehydration, and part of the Fe_3O_4-CNT complex could also bind to the outer wall of the composite microbubble. Thus, most of the Fe_3O_4-CNT complexes existed on the outside of the microbubble. Additionally, a small amount of the Fe_3O_4-CNT complex could be encapsulated inside the composite microbubble under acoustic vibration.

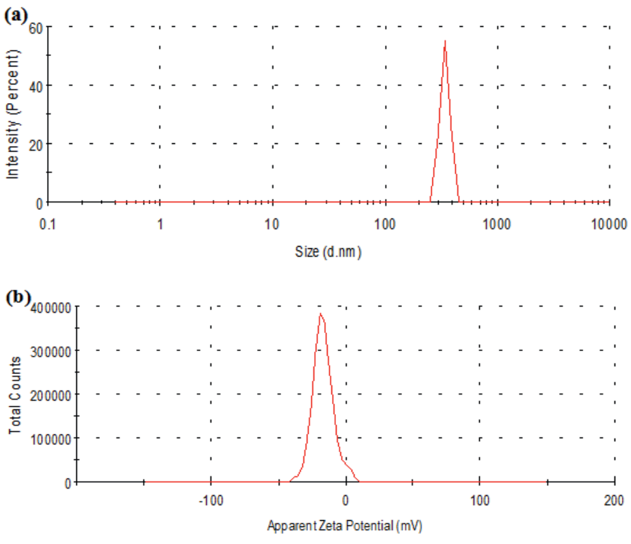

Fig. 3 Size (a) and zeta potential (b) of Span-PEG-composited Fe_3O_4-CNT microbubbles.

Fig. 3 shows the particle size distribution and zeta potential of Span-PEG-composited Fe_3O_4-CNT microbubbles. The size of the composite microbubbles was uniform, the average particle size was 425 nm, and the particle size distribution manifested as the unimodal form (Fig. 3). The zeta potential was −27.5 mV, indicating that the composite microbubbles had good stability and met the requirements as an ultrasound contrast agent.

To detect the ASA load rate in Span-PEG-composited Fe_3O_4-CNT-ASA microbubbles, the ASA standard curve (Fig. 4) and ASA absorbance in composite microbubbles (Table 1) were obtained according to the experimental method in Section 2.2.1 of this study. Thus, the ASA load rate in Span-PEG-composited Fe_3O_4-CNT-ASA microbubbles was 1.12%. Similarly, the GM standard curve (Fig. 5) and GM absorbance in composite microbubbles (Table 2) were obtained according to the experimental method

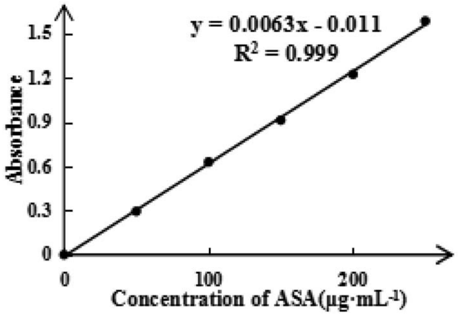

Fig. 4 Standard curve for ASA.

Table 1 ASA absorbance in the composite microbubbles ($n = 5$)

Times	1	2	3	4	5	Average
ASA absorbance	0.112	0.150	0.099	0.156	0.132	0.130
ASA loading rate (%)	0.97	1.28	0.88	1.32	1.14	1.12

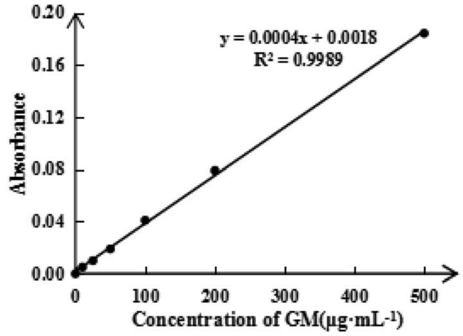

Fig. 5 Standard curve for GM.

in section 2.2.2 of this study. The GM load rate in Span-PEG-composited Fe_3O_4-CNT-GM microbubbles was calculated as 19.05%.

Fig. 6 shows the inhibitory effects of Span-PEG-composited Fe_3O_4-CNT-GM microbubbles in different concentrations on *Escherichia coli* and *Staphylococcus aureus*. The inhibitory effect of the composite microbubbles on *Escherichia coli* and *Staphylococcus aureus* showed a concentration-dependent trend; its bacteriostatic effect gradually increased as the concentration of the composite microbubbles increased (Fig. 6). Specifically, for *Escherichia coli*, the concentration of Span-PEG-composited Fe_3O_4-CNT-GM microbubbles was 0 mg mL^{-1} and the diameter of the inhibition zone was 6.9 ± 0.2 mm. When the concentration was 20–40 mg mL^{-1}, the diameter range was 10.5 ± 0.5–13.4 ± 0.8 mm, indicating medium drug sensitivity. When the concentration was 60–80 mg mL^{-1}, the diameter range was 16.8 ± 0.9–19.7 ± 0.4 mm, indicating high drug sensitivity. Additionally, when the concentration was $>$ 80 mg mL^{-1}, the drug sensitivity was extremely sensitive. For *Staphylococcus aureus*, when the concentration of Span-PEG-composited Fe_3O_4-CNT-GM microbubbles was 20 mg mL^{-1}, the diameter of the inhibition circle was 9.6 ± 0.4 mm, indicating low drug sensitivity. When the concentration was 40–60 mg mL^{-1}, the diameter range was 11.7 ± 0.8–14.4 ± 0.7 mm, indicating medium drug sensitivity. Additionally, when the concentration $>$ 80 mg mL^{-1}, high drug sensitivity was noted. In summary, the antibacterial effect of Span-PEG-composited Fe_3O_4-CNT-GM microbubbles on *Escherichia coli* and *Staphylococcus aureus* was dose-dependent, and the inhibitory effect on *Escherichia coli* was higher than that of *Staphylococcus aureus*. When the concentration of Span-PEG-composited Fe_3O_4-CNT-GM microbubbles reached 60 mg mL^{-1} or higher, both bacteria demonstrated favorable antibacterial effects.

Table 2 GM absorbance in the composite microbubble ($n = 5$)

Times	1	2	3	4	5	Average
GM absorbance	0.070	0.076	0.088	0.072	0.083	0.078
GM loading rate (%)	16.98	18.58	21.66	17.61	20.37	19.05

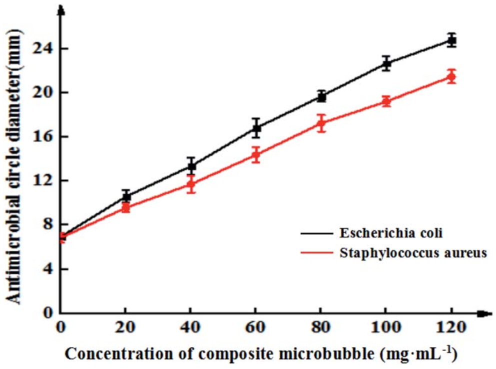

Fig. 6 Inhibition curves of Span-PEG-composited Fe_3O_4-CNT-GM microbubbles at different concentrations for the effect on *Escherichia coli* and *Staphylococcus aureus*.

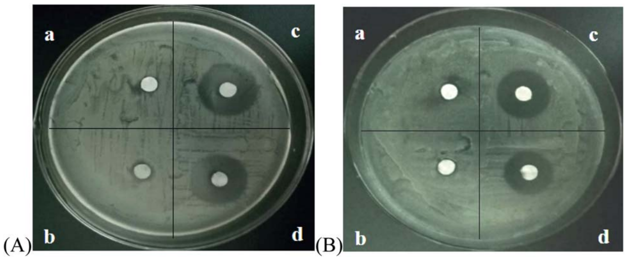

Fig. 7 Antibacterial activity of different microbubbles on (A) *Escherichia coli* and (B) *Staphylococcus aureus*. (a) Span-PEG microbubbles. (b) Span-PEG-composited Fe_3O_4-CNT microbubbles. (c) Span-PEG-composited CNT-GM microbubbles. (d) Span-PEG-composited Fe_3O_4-CNT-GM microbubbles.

The antimicrobial effects of the different microbubbles on *Escherichia coli* and *Staphylococcus aureus* are shown in Fig. 7. Span-PEG microbubbles and Span-PEG-composited Fe_3O_4-CNTs demonstrated no antibacterial activity. Span-PEG-composited CNT-GM microbubbles and Span-PEG-composited Fe_3O_4-CNT-GM microbubbles manifested good antibacterial activity against *Escherichia coli* and *Staphylococcus aureus*, and their bacteriostatic activity on *Escherichia coli* was stronger.

The bacteriostatic circle diameters of different composite microbubbles on *Escherichia coli* and *Staphylococcus aureus* are shown in Table 3. For *Escherichia coli*, the bacteriostatic circle diameter of the Span-PEG microbubble group was 6.8 ± 0.42 mm and that of the Span-PEG-composited Fe_3O_4-CNT microbubble group was 7.2 ± 0.56 mm, with no significant difference between the groups ($P > 0.05$). Span-PEG-composited CNT-GM microbubbles (21.2 ± 1.02 mm) showed a significant difference compared with Span-PEG microbubbles ($P < 0.01$),

Table 3 Inhibitory effect of the different composite microbubbles ($\bar{x} \pm s$)[a]

	Diameter of the bacteriostatic circle D mm^{-1}	
Group	*Escherichia coli*	*Staphylococcus aureus*
Span-PEG microbubbles	6.8 ± 0.42	6.5 ± 0.3
Span-PEG-composited Fe_3O_4-CNTs microbubbles	7.2 ± 0.56	6.4 ± 0.35
Span-PEG-composited CNT-GM microbubbles	$21.2 \pm 1.02^{\#}$	$18.1 \pm 0.73^{\#}$
Span-PEG-composited Fe_3O_4-CNT-GM microbubbles	$18.6 \pm 0.81^{\#}$	15.8 ± 0.65*

[a] "*" for $P < 0.05$,"#" for $P < 0.01$.

and Span-PEG-composited Fe_3O_4-CNT-GM microbubbles (18.6 ± 0.81 mm) also showed a significant difference compared with Span-PEG microbubbles ($P < 0.01$). For *Staphylococcus aureus*, Span-PEG microbubbles and Span-PEG-composited Fe_3O_4-CNT microbubbles showed no antibacterial activity. The diameter of the bacteriostatic circle of Span-PEG-composited CNT-GM microbubbles was 18.1 ± 0.73 mm, showing a significant difference compared with Span-PEG microbubbles ($P < 0.01$). The diameter of the Span-PEG-composited Fe_3O_4-CNT-GM microbubbles was 15.8 ± 0.65 mm, showing a significant difference compared with Span-PEG microbubbles ($P < 0.05$). In summary, Span-PEG membrane material and Fe_3O_4-CNTs as the targeted drug carrier showed no bacteriostatic activity. Both Span-PEG-composited CNT-GM microbubbles and Span-PEG-composited Fe_3O_4-CNT-GM microbubbles exhibited good antibacterial activity on *Escherichia coli* and *Staphylococcus aureus*, indicating that the antibacterial effect of Span-PEG-composited Fe_3O_4-CNT-GM microbubbles originated from the loading drug GM, and the inhibitory effects of Span-PEG-composited CNT-GM microbubbles and Span-PEG-composited Fe_3O_4-CNT-GM microbubbles on *Escherichia coli* were better than those on *Staphylococcus aureus*.

The thrombosis inhibition results of Span-PEG-composited Fe_3O_4-CNT-ASA microbubbles with different concentrations are shown in Table 4. With the increase in the composite microbubble concentration, the wet and dry weights of the thrombus were both reduced. When the concentration of Span-PEG-composited Fe_3O_4-CNT-ASA was from 40 mg mL^{-1} to 80 mg mL^{-1}, the wet weight and dry weight of the thrombus showed little change, with no statistical significance ($P > 0.05$) compared with the concentration at 0 mg mL^{-1}. When the concentration of Span-PEG-composited Fe_3O_4-CNT-ASA microbubbles was 120 mg mL^{-1}, a significant difference was found in the wet and dry weights of the thrombus compared with that at the concentration of 0 mg mL^{-1} ($P < 0.05$), indicating that the composite microbubbles inhibited the thrombosis *in vitro* at this time. When the concentration of Span-PEG-composited Fe_3O_4-CNT-ASA microbubbles was 160 mg mL^{-1}, the wet weight of the thrombus was significantly different from that at 0 mg mL^{-1} ($P < 0.05$), and the dry weight of the thrombus showed a very significant difference compared with that at 0 mg mL^{-1} ($P < 0.05$). When the concentration of Span-PEG-composited Fe_3O_4-CNT-ASA microbubbles was 200 mg mL^{-1}, the wet and dry weights of the thrombus were significantly different from those at 0 mg mL^{-1} ($P < 0.05$). Thus, Span-PEG-composited Fe_3O_4-CNT-ASA microbubbles inhibit thrombosis *in vitro* and show a dose-dependent trend.

The thrombosis inhibition effects *in vitro* for different microbubble groups at the concentration of 120 mg mL^{-1} and the normal saline group are shown in Table 5. The wet and dry weights of the thrombus in the saline control group were 128.43 ± 8.11 mg and 50.27 ± 1.33 mg, respectively. Those of the Span-PEG microbubble group and Span-PEG-composited Fe_3O_4-CNT microbubble group were not statistically significant compared with those of the control group ($P > 0.05$), indicating that Span-PEG membrane material and the Fe_3O_4-CNT targeted drug-loading complex could not inhibit the thrombosis *in vitro*. The wet and dry weights of the thrombus for Span-PEG-composited CNT-ASA microbubbles showed a very significant difference compared with those of the saline control group ($P < 0.01$). Compared with the control group, the wet and dry weights of the thrombus for Span-PEG-composited Fe_3O_4-CNT-ASA

Table 4 Inhibitory effect of Span-PEG-composited Fe_3O_4-CNT-ASA microbubbles at different concentrations on thrombosis ($\bar{x} \pm s$)[a]

Number	Concentration of composite microbubbles (mg mL^{-1})	Wet weight of thrombus (mg)	Dry weight of thrombus (mg)
1	0	126.17 ± 10.90	53.60 ± 6.95
2	40	122.63 ± 12.22	51.00 ± 9.54
3	80	105.30 ± 9.54	39.70 ± 2.29
4	120	93.93 ± 13.40*	36.17 ± 6.67*
5	160	84.37 ± 11.14*	$25.87 \pm 4.85^{\#}$
6	200	$63.10 \pm 9.88^{\#}$	$18.33 \pm 5.82^{\#}$

[a] "*" for $P < 0.05$,"#" for $P < 0.01$.

Table 5 Inhibition effect of different composite microbubbles on thrombosis *in vitro* ($\bar{x} \pm s$)[a]

Group	Wet weight of thrombus (mg)	Dry weight of thrombus (mg)
Normal saline	128.43 ± 8.11	54.97 ± 5.04
Span-PEG microbubbles	121.30 ± 3.99	50.27 ± 1.33
Span-PEG-composited Fe_3O_4-CNTs microbubbles	123.00 ± 8.41	53.10 ± 7.31
Span-PEG-composited CNT-ASA microbubbles	92.43 ± 6.64[#]	32.30 ± 5.31[#]
Span-PEG-composited Fe_3O_4-CNT-ASA microbubbles	97.97 ± 8.97*	36.00 ± 4.80[#]

[a] Compared with the normal saline control group, "*" for $P < 0.05$,"[#]" for $P < 0.01$.

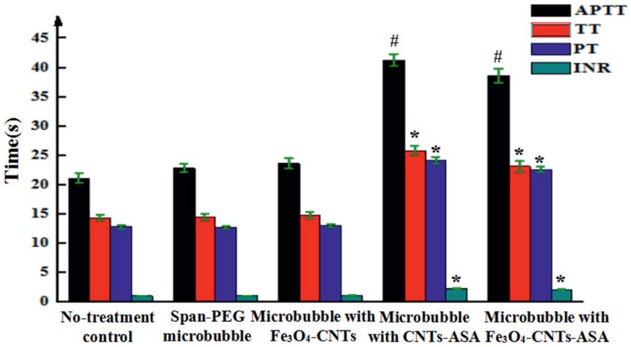

Fig. 8 Anticoagulation effect of different composite microbubbles *in vitro*.

microbubbles showed significant differences ($P < 0.05$ and $P < 0.01$, respectively). Span-PEG-composited CNT-ASA microbubbles and Span-PEG-composited Fe_3O_4-CNT-ASA microbubbles could effectively inhibit the thrombosis *in vitro*, and this inhibition effect was mainly derived from the drug ASA in the composite microbubbles. No significant difference was found between the wet and dry weights of the thrombus for Span-PEG-composited CNT-ASA microbubbles and Span-PEG-composited Fe_3O_4-CNT-ASA microbubbles, indicating the effect of Fe_3O_4 particles on the CNT surface on the drug loading performance of CNTs was not obvious.

Fig. 8 shows the coagulation indexes of different composite microvesicles. APTT, TT, PT, and INR are commonly used to determine the coagulation index. APTT reflects the total coagulation status of each coagulation component in the endogenous coagulation system. PT and INR reflect the coagulation status of the exogenous coagulation system, and TT reflects the coagulation status of plasma fibrinogen converting into fibrin. Span-PEG microbubbles and Span-PEG-composited Fe_3O_4-CNT microbubbles did not influence APTT, TT, PT, and INR, with no statistical significance compared with the control group (Fig. 8; $P > 0.05$). Span-PEG-composited CNT-ASA microbubbles and Span-PEG-composited Fe_3O_4-CNT-ASA microbubbles significantly increased the value of APTT, which was significantly different from that of the control group ($P < 0.01$), indicating that the two composite microbubbles affect the endogenous coagulation system. At the same time, Span-PEG-composited CNT-ASA microbubbles and Span-PEG-composited Fe_3O_4-CNT-ASA microbubbles increased the values of TT, PT, and INR, which were significantly different from those of the control group ($P < 0.05$), indicating that these two microbubbles had a good effect on the exogenous coagulation system and the conversion of plasma fibrinogen to fibrin. An INR value at the range of 2.1–3 indicates moderate anticoagulation. The INR values of Span-PEG-composited CNT-ASA microbubbles and Span-PEG-composited Fe_3O_4-CNT-ASA microbubbles were 2.23 and 2.15, respectively, indicating that the prepared Span-PEG-composited Fe_3O_4-CNT-ASA microbubbles demonstrated anticoagulant activity and could play a role in adjuvant therapy.

The ultrasound imaging effect of Span-PEG-composited Fe_3O_4-CNT-GM microbubbles in the rabbit uterus is shown in Fig. 9. Before perfusion of the composite microbubbles (Fig. 9(a)), the uterus was not displayed in the ultrasound image because the echo signal was weak, leading to a challenging ultrasound diagnosis of the uterine lesion. After perfusion of the composite microbubbles, the uterus shape was clear and a strong echo existed across the entire uterus. Moreover, no obvious resistance and no reflux during the injection were detected; the composite microbubbles could easily flow throughout the uterus. The composite microbubbles showed good stability and fluidity and generated strong sound scattering. Thus, the image contrast increased and effective imaging was achieved.

Fig. 10 displays the ultrasound imaging results of a rabbit aortic thrombus after the injection of normal saline, Span-PEG microbubbles, Span-PEG-composited CNT microbubbles and Span-PEG-composited Fe_3O_4-CNT-ASA microbubbles. The echo signal was very low, and the obtained imaging contrast was low for the saline group, making it impossible to effectively diagnose the lesion (Fig. 10(a)). The imaging clarity was enhanced because the blood appeared as a low-density echo signal, and effective imaging of the Span-PEG microbubble group was

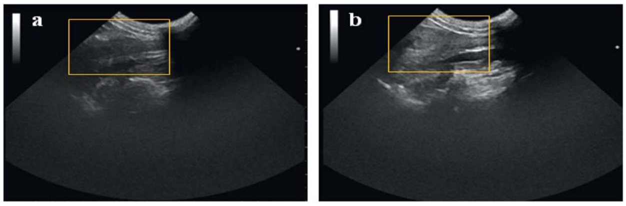

Fig. 9 Ultrasonic imaging effect of the rabbit uterus before (a) and after (b) perfusion with Span-PEG-composited Fe_3O_4-CNT-GM microbubbles.

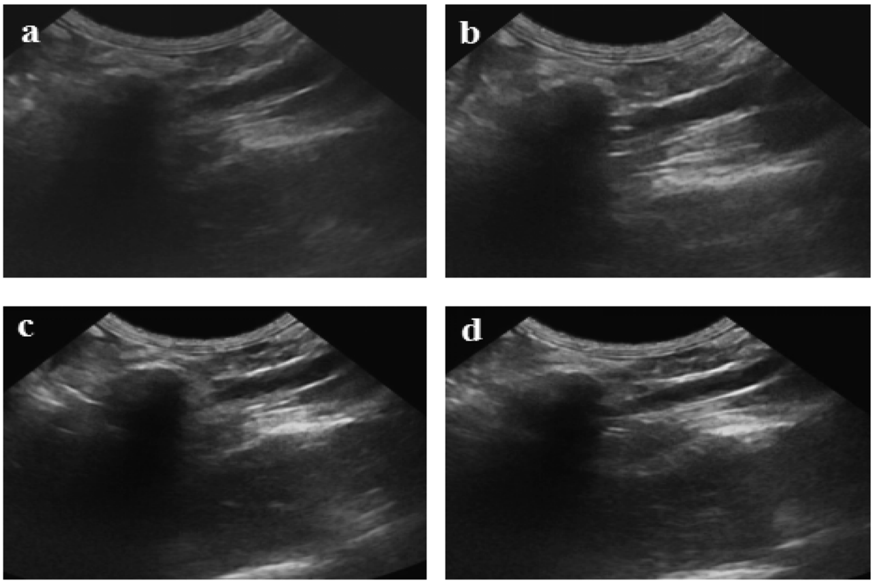

Fig. 10 Ultrasound imaging of the rabbit abdominal aorta after the infusion of different contrast agents. (a) Saline. (b) Span-PEG microbubbles. (c) Span-PEG-composited CNT microbubbles. (d) Span-PEG-composited Fe_3O_4-CNT-ASA microbubbles.

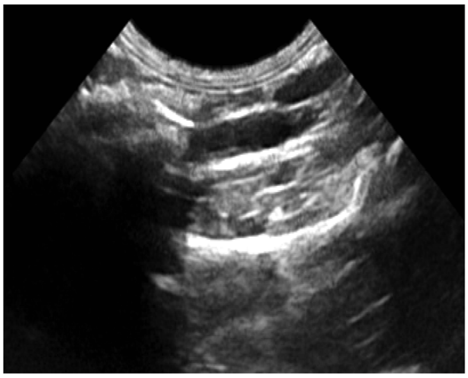

Fig. 11 Ultrasound imaging of the rabbit abdominal aorta after the instillation of Span-PEG composite Fe_3O_4-CNT-ASA microvesicles in an external magnetic field.

achieved (Fig. 10(b)). Fig. 10(c) represents the ultrasound imaging of the rabbit abdominal aorta after the injection of Span-PEG-composited CNT microbubbles. After a few seconds of injection, the blood vessels of the rabbit abdominal aorta rapidly filled up and the echo signal rapidly brightened; the enhanced contrast effect was more evident than that of Span-PEG microbubbles. For Span-PEG-composited Fe_3O_4-CNT-ASA microbubbles (Fig. 10(d)), the blood vessels of the abdominal aorta rabbit rapidly filled up after a few seconds of injection, and the signal rapidly increased and became brighter. The ultrasound signal of Span-PEG-composited Fe_3O_4-CNT-ASA microbubbles was similar to that of Span-PEG-composited CNT microbubbles, and the thrombosis location of the abdominal aorta was clear. Thus, Span-PEG-composited Fe_3O_4-CNT-ASA microbubbles could effectively diagnose the lesion.

Fig. 11 shows ultrasound imaging of the rabbit abdominal aorta in an external magnetic field for Span-PEG-composited Fe_3O_4-CNT-ASA microbubbles. The blood vessels of the rabbit abdominal aorta quickly filled up after a few seconds of injection, and Span-PEG-composited Fe_3O_4-CNT-ASA microbubbles aggregated under the action of an external magnetic field because of Fe_3O_4 as a magnetic targeting factor, causing the signal to gradually increase and effectively extending the time of ultrasound imaging (Fig. 11). Compared with the non-applied magnetic field (Fig. 10(d)), the obtained ultrasound image had higher contrast. Thus it can be seen that the Fe_3O_4 particles on Fe_3O_4-CNT complex played a very good magnetic targeting role. Additionally, it was sufficient to meet the clinical requirements for the contrast time of ultrasound contrast agents. The above results indicated that the prepared Span-PEG-composited Fe_3O_4-CNT-ASA microbubbles could achieve targeted ultrasound imaging of thrombosis under the action of an external magnetic field.

4 Conclusion

In this study, Span-PEG-composited Fe_3O_4-CNTs, a new multifunctional microbubble type, were designed and prepared by an *in situ*, liquid-phase synthesis method and acoustic cavitation. Here, CNT was used as the carrier of the magnetic targeting factor and drug loading, the magnetic targeting complex Fe_3O_4-CNT was respectively loaded with ASA and GM. The obtained composite microbubbles could realize targeted ultrasound imaging and adjuvant therapy for thrombosis and inflammation. We believe that this new multifunctional ultrasound contrast agent will have a good application prospect.

Conflicts of interest

There are no conflicts to declare.

Acknowledgements

This work was supported by the National Natural Science Foundation of China (No. 51671096 and 81601616), Scientific Research Initiation Found of Postdoctoral Researchers Settled down in Heilongjiang (31303120), Excellent Innovation Team based on the basic scientific research vocational cost for the provincial undergraduate Universities in Heilongjiang (No. 2018-KYYWF-0914) and Heilongjiang Health Department Project (2019-291).

References

1 D. Hyun, L. Abou Elkacem, R. Bam, *et al.*, Nondestructive Detection of Targeted Microbubbles Using Dual-Mode Data and Deep Learning for Real-Time Ultrasound Molecular Imaging, *IEEE Trans. Med. Imag.*, 2020, (2), 3079–3088.

2 Y. Zhang, Y. Zhong, M. Ye, *et al.*, Polydopamine-modified dual-ligand nanoparticles as highly effective and targeted magnetic resonance/photoacoustic dual-modality thrombus imaging agents, *Int. J. Nanomed.*, 2019, **14**, 7155–7171.

3 N. Beziere, C. von Schacky, Y. Kosanke, *et al.*, Optoacoustic Imaging and Staging of Inflammation in a Murine Model of Arthritis, *Int. J. Nanomed.*, 2014, **66**(8), 2071–2078.

4 G. Lippi, M. Franchini and G. Targher, Arterial thrombus formation in cardiovascular disease, *Nat. Rev. Cardiol.*, 2011, **8**(9), 502–512.

5 S. P. Jackson, Arterial thrombosis–insidious, unpredictable and deadly, *Nat. Med.*, 2011, **17**(11), 1423–1436.

6 M. Di Nisio, N. van Es and H. R. Büller, Deep vein thrombosis and pulmonary embolism, *Lancet*, 2016, **388**(10063), 3060–3073.

7 A. Johri, T. Li, O. Yau, *et al.*, Novel Ultrasound Methods to Investigate Carotid Artery Plaque Vulnerability, *J. Am. Soc. Echocardiogr.*, 2017, **30**(2), 139–148.

8 D. Kim, R. Joukje van, M. Velja, *et al.*, Oil-Based or Water-Based Contrast for Hysterosalpingography in Infertile Women., *N. Engl. J. Med.*, 2017, **376**(21), 2043–2052.

9 R. Zhang, Z. Liu, Y. Luo, *et al.*, Tri-stimuli responsive carbon nanotubes covered by mesoporous silica graft copolymer multifunctional materials for intracellular drug delivery, *J. Ind. Eng. Chem.*, 2019, **80**, 431–443.

10 E. Attari, H. Nosrati, H. Danafar, *et al.*, Methotrexate anticancer drug delivery to breast cancer cell lines by iron oxide magnetic based nanocarrier, *J. Biomed. Mater. Res., Part A*, 2019, **107**(11), 2492–2500.